Alexey Slunyaev
Institute of Applied Physics,
Nizhny Novgorod, Russia;
N. Novgorod State Technical University,
Nizhny Novgorod, Russia
e-mail: slunyaev@hydro.appl.sci-nnov.ru

Efim Pelinovsky
Institute of Applied Physics,
Nizhny Novgorod, Russia;
N. Novgorod State Technical University,
Nizhny Novgorod, Russia; and
National Research University – Higher
School of Economics,
Nizhny Novgorod, Russia
e-mail: pelinovsky@hydro.appl.sci-nnov.ru

C. Guedes Soares
Centre for Marine Technology and Engineering,
(CENTEC), Technical University of Lisbon,
Instituto Superior Tecnico,
1049-001 Lisboa, Portugal
e-mail: guedess@mar.ist.utl.pt

Reconstruction of Extreme Events Through Numerical Simulations

In this paper, some abnormal or rogue wave events registered in the North Sea by means of the surface elevation measurements are reconstructed with the help of theoretical models for water waves and numerical simulations of wave evolution. Time series of surface elevation, which are measured at a single point, provide incomplete information about the waves. The registered time series are used to restore the wave dynamics under reasonable assumptions. Different frameworks associated with the relation between the surface elevation and the fluid velocity fields are considered, and different numerical models are used to simulate the wave dynamics in time and space. It is shown that for some abnormal or rogue wave records the result of the extreme event reconstruction is robust. In particular, the verification of approximate approaches versus the fully nonlinear numerical simulation is performed. The reconstructed rogue wave is generally less steep than the measured one. Possible reasons for this discrepancy are suggested.
[DOI: 10.1115/1.4025545]

Keywords: rogue waves, in situ registration, numerical simulations, wave envelopes, extreme event reconstruction

1 Introduction

The popularity of abnormal, freak, or rogue wave problem amplified suddenly within the last few decades, and it is nowadays a top-rank topic for scientific discussions, conferences, and publications in marine science [1–3]. The problem has motivated theoreticians, who managed to reveal new extraordinary features in the nonlinear wave dynamics, and naval architects and marine engineers thanks to trustworthy testimonies of the ultimate effects caused by these extreme waves. Most frequently, rogue waves are specified with the help of a simple amplitude criterion, so that a wave is assumed *rogue*, if its height at least twice larger than the significant wave height. At the same time, the discussion on a proper selection of this wave popularity is still open.

Already, there is a number of well-documented cases of occurrence of unexpectedly large sea waves. It is well understood that the sea may be dangerous for navigation. It is also commonly expected that the modern engineering level of knowledge is high enough to protect people from many disasters.

Today, observations and measurements of high waves from space become possible. A three-week registration of surface waves from the European satellite ERS-2 revealed the regions with high waves and detected a wave of 29.8 m height [4]. Bearing in mind that ships are often designed for 10–15 m wave heights, it becomes obvious that the observed waves are real threats that may cause damage and the ship lost.

The state of affairs can always be improved and casualties can be reduced in frequency and consequences. Hundreds of vessels sink and hundreds of people perish annually, although the situation takes a turn for the better through years [5]. The list of accidents related to the attacks of huge waves contains many recent dates. Thus, 22 super carriers were lost or severely damaged between 1969 and 1994 due to the occurrence of sudden rogue waves; a total of 542 lives were lost as a result [6].

During incidents, relatively high waves are expected to be recorded. Toffoli et al. [7] found, however, that rather low significant wave heights occurred during those ship accidents, which have been reported as being due to bad weather. Thus, this could suggest that the significant wave height is not the only governing factor that leads to accidents. In fact, Guedes Soares et al. [8] studying accidents reported during a reasonable period in the North Atlantic demonstrated that the areas of larger heavy weather accident rates coincide with the areas of larger mean wave steepness [9], what may claim the importance of wave nonlinearity effects.

The wave loading on stationary or moving floating structures may be determined by other parameters than wave height, such as steepness, crest height, horizontal wave asymmetry; in particular wave sequences are also expected to be quite dangerous due to the memory and resonance effects [10]. Different types of ships will be prone to different wave parameters and conditions. Different kinds of extreme waves may be treated as rogues wave or not, depending on particular cases and applications. This is an important practical question, which should be answered.

The present work aims at reproducing realistic extreme sea wave events, related to *abnormal, rogue* or *freak* waves, which were registered in the ocean by means of records of the surface elevation time series. Having this information only at one point in space is in fact ambiguous, but it is still very useful, and attractive. The measured time series retains the information on wave dynamics hidden. When the wave evolution is known, the features associated with the rogue wave may be computed, and the important characteristic of the dangerous incident, the rogue wave lifetime, may be estimated.

In most cases, the surface elevation at a single point is available, although the surface wave represents a combination of the surface movement and the fluid movement within the water column. Obtaining the water velocity field is the first problem when one desires to estimate the wave dynamics.

In some simplified cases the relation between the surface elevation and the water velocity is known from the theory. To do so the waves are generally supposed to be unidirectional. Then, they are often assumed to be weakly nonlinear or/and narrow-banded. However, realistic rogue waves are extreme, they are strongly nonlinear and have broad spectrum thus the approaches listed above are not verified, and their capability to describe the case is not obvious.

The wave envelope (wave modulations) concept is a particular case when the surface elevation and the water field velocity are

Contributed by the Ocean, Offshore, and Arctic Engineering Division of ASME for publication in the Journal of Offshore Mechanics and Arctic Engineering. Manuscript received June 5, 2012; final manuscript received July 15, 2013; published online November 12, 2013. Assoc. Editor: Elzbieta Maria Bitner-Gregersen.

related in a straightforward way, so that the evolution equations have a relatively simple form and govern the dynamics of complex wave amplitude. Recently, this approach was shown able to describe rather well even quite steep and short nonlinear wave packets [11–15].

The reproduction of wave temporal and spatial dynamics was probably first performed by Trulsen [16] numerically for the case of the well-known New Year Wave record (retrieved at the Draupner platform in the North Sea), within the framework of envelope equations (a modified Dysthe model, see Refs. [17–20]). This and other extreme wave events were reproduced in laboratory conditions by Clauss and Klein (see Ref. [21], and references therein) with the help of an iterative procedure on the basis of the "nonlinear" dispersive law for Stokes waves.

Several rogue wave records from the North Sea and Black Sea were simulated by means of the envelope models (the nonlinear Schrödinger and the Dysthe equations) in Refs. [22–24]; there the lifetime of the abnormal wave events was estimated as long as up to about 100 sec. The present paper reports on the further development of that research, with combination of temporal and spatial evolution approaches, application of different envelope concepts and the use of strongly nonlinear simulations.

Rogue waves were registered from the North Alwyn fixed steel jacket platform in the northern North Sea (1°44′ E 60°45′ N, depth 126 m) during the storm from the 16th to 22nd of Nov. 1997. During this storm several abnormal waves were identified as reported in Ref. [25]. Four records NA9711180110, NA9711200131, NA9711200151, and NA9711200311 were studied in Ref. [23] (the codes contain the year, month and time of the registration); six other records NA9711161053, NA9711190751, NA9711191831, NA9711192011, NA9711192351, and NA9711200731 were considered in less details in Ref. [24]. These ten time series are examined in the present study. It is shown that some of them may be sufficiently well described within the approximate Dysthe model approach, and the strongly nonlinear effects generally result in the sharper single wave profile. However, this approach seems to be capable of describing the extreme wave evolution up to about 10 min, but fails to describe the whole 20-min time series. Some of the extreme wave records from the North Alwyn could not be reproduced with acceptable accuracy by means of the envelope approach.

In Sec. 2, an overview of the numerical models employed is given. The problem of reconstruction of the fluid velocity for given surface elevation is discussed in Sec. 3. Section 4 presents the results of numerical reconstructions of rogue wave dynamics, including the results of fully nonlinear wave simulations. Closing words and results are formulated in Sec. 5.

2 Numerical Models

Theoretical models that describe the unidirectional propagation of surface gravity potential waves over deep water are employed in the present study, the high order spectral method for solution of the Euler equations, and the modified nonlinear Schrödinger theory.

2.1 Primitive Equations of Potential Hydrodynamics. The primitive equations of the potential hydrodynamics for the surface displacement $\eta(x,t)$ and the surface velocity potential $\Phi(x,t)=\varphi(x,t,z=\eta)$ have the form

$$\frac{\partial \eta}{\partial t}=-\frac{\partial \Phi}{\partial x}\frac{\partial \eta}{\partial x}+\left(1+\left(\frac{\partial \eta}{\partial x}\right)^2\right)\frac{\partial \varphi}{\partial z} \tag{1}$$

$$\frac{\partial \Phi}{\partial t}=-g\eta-\frac{1}{2}\left(\frac{\partial \Phi}{\partial x}\right)^2+\frac{1}{2}\left(\frac{\partial \varphi}{\partial z}\right)^2\left[1+\left(\frac{\partial \eta}{\partial x}\right)^2\right] \tag{2}$$

$$\frac{\partial^2 \varphi}{\partial x^2}+\frac{\partial^2 \varphi}{\partial z^2}=0,\quad z\le\eta \tag{3}$$

$$\frac{\partial \varphi}{\partial z}\to 0,\quad z\to-\infty \tag{4}$$

Here, x is the spatial coordinate along the wave propagation, and t is time. The Oz axis is directed upward, and g is the acceleration due to gravity.

Equations (1) and (2) constitute the surface boundary condition. Equation (3) is the Laplace equation for the velocity potential, and Eq. (4) is the bottom condition (an infinitively deep water case is considered).

Equations (1)–(4) are integrated in time by means of the high-order spectral method (HOSM) in the method presented in Ref. [26]. Following this approach, the Laplace equation for velocity potential, Eq. (3), is solved in a fixed domain, where the curved free boundary at the water surface is substituted by a horizontal line $z=0$. The velocity potential, $\varphi(x,z,t)$, is represented in the form of a Taylor series of a given order (characterized by parameter M) around the rest water level, what allows obtaining its value at the surface, $\Phi(x,t)$.

The HOSM is strictly speaking not a fully-nonlinear, but a strongly nonlinear algorithm, which resolves the wave-wave interactions up to the predetermined order M (for $M=3$ this approach is of the same accuracy as the Zakharov equation [27]). The value $M=6$ of the parameter is used in the present study, what corresponds to practically *fully nonlinear* case (see discussion in Ref. [28]).

2.2 Equations for Wave Modulations. The primitive hydrodynamic equations are difficult for analysis and even for solving numerically; therefore, approximate approaches are popular. The envelope approach which is very powerful, describes the wave fields in terms of one complex function, the wave amplitude; and the dynamical equations describe wave modulations (narrow-banded wave assumption).

The simplest theory on this way is represented by the nonlinear Schrödinger (NLS) equation, which may be written in form

$$i\left(\frac{\partial A}{\partial t}+C_{gr}\frac{\partial A}{\partial x}\right)+\frac{\omega_0}{8k_0^2}\frac{\partial^2 A}{\partial x^2}+\frac{\omega_0 k_0^2}{2}\left|A\right|^2 A=0 \tag{5}$$

Here $A(x,t)$ is the complex wave amplitude. Parameters ω_0 and k_0 are the mean cyclic frequency and wavenumber, respectively, linked by the deep-water dispersion relation

$$\omega^2=kg \tag{6}$$

$C_{gr}=d\omega/dk$ denotes the group velocity for specified k_0.

When the first two terms in Eq. (5) prevail, linear effects are dominant. If the two first and the last terms in Eq. (5) are the main players, then the group nonlinearity is the most important, and the nonlinear self-modulation due to the Benjamin–Feir instability develops, see Ref. [27].

In fact, the NLS equation (5) is capable of describing moderately nonlinear waves only for a few periods; thus, it is not sufficient if one needs to consider a long distance or steep waves. Besides the NLS equation, the improved theory for wave modulations is employed in this study, the modifications of the Dysthe model [18–20,29]. This framework takes into account the next-order terms of nonlinear dispersion, and the full linear dispersion

$$i\frac{\partial A}{\partial t}+\hat{L}\left[\frac{\partial}{\partial x}\right]A+\frac{\omega_0 k_0^2}{2}\left|A\right|^2 A+i\frac{3\omega_0 k_0}{2}\left|A\right|^2\frac{\partial A}{\partial x}+i\frac{\omega_0 k_0}{4}A^2\frac{\partial A^*}{\partial x}+k_0 A\frac{\partial \bar{\phi}}{\partial x}=0 \tag{7}$$

$$\frac{\partial \bar{\varphi}}{\partial z}=\frac{\omega_0}{2}\frac{\partial}{\partial x}\left|A\right|^2,\quad z=0 \tag{8}$$

The function $\bar{\varphi}$ is the induced long-scale flow, which should satisfy Eqs. (3) and (4). The long-scale velocity potential at the rest

water level is $\bar{\phi} = \bar{\varphi}(z = 0)$. The operator $\hat{L}$ in Eq. (7) acts in the Fourier space and provides fulfillment of the exact water-wave dispersion law, Eq. (6), for all wavenumbers (see details in Refs. [18,20]).

The complex envelope $A(x,t)$ describes both the surface displacement and the velocity potential, what is done by virtue of the following third-order asymptotic formulas (according to Refs. [20,29]).

$$\eta(x,t) = \bar{\eta} + \eta^{(1)} + \eta^{(2)} + \eta^{(3)} \tag{9}$$

$$\bar{\eta} = \frac{1}{2\omega}\frac{\partial\bar{\phi}}{\partial x}$$

$$\eta^{(1)} = \mathrm{Re}(AE), \quad \eta^{(2)} = \frac{k_0}{2}\mathrm{Re}\left(A^2E^2\right),$$

$$\eta^{(3)} = -\frac{1}{2}\mathrm{Im}\left(A\frac{\partial A}{\partial x}E^2\right) + \frac{3k_0^2}{8}\mathrm{Re}\left(A^3E^3\right)$$

$$\varphi(x,z,t) = \bar{\varphi} + \varphi^{(1)} + \varphi^{(2)} + \varphi^{(3)} \tag{10}$$

$$\varphi^{(1)} = -\frac{\omega_0}{k_0}\mathrm{Im}(AE)e^{k_0z}$$

$$\varphi^{(2)} = \frac{\omega_0}{2k_0^2}\mathrm{Re}\left[\frac{\partial A}{\partial x}E\right](1-2kz)e^{k_0z}$$

$$\varphi^{(3)} = \frac{\omega_0k_0}{8}\mathrm{Im}\left[A\left|A\right|^2E\right]e^{k_0z} + \frac{\omega_0}{8k_0^3}\mathrm{Im}\left[\frac{\partial^2A}{\partial x^2}E\right]\left(3-4kz+4k^2z^2\right)e^{k_0z}$$

$$E \equiv \exp(i\omega_0t - ik_0x)$$

Limiting cases of reconstruction formulas, Eqs. (9) and (10), agree with expressions for the fluid velocities in Refs. [19,20]. The induced mean flow $\bar{\varphi}(x,t,z)$ is obtained through numerical solution of the Laplace equation with use of the boundary conditions, Eqs. (4) and (8).

The asymptotic Dysthe model has the benefit of easy transformation from the form, Eqs. (7)–(8), which governs the evolution in time (t-evolution) to the one, which describes the evolution in space (x-evolution). This trick is based on the asymptotic approach implying weak nonlinearity and dispersion, so that in the leading order the wave evolution is supposed to be described by the wave equation. The spatial form of the Dysthe equation (7) has the form

$$i\left(\frac{\partial A}{\partial x} + \frac{1}{C_{gr}}\frac{\partial A}{\partial t}\right) + \frac{k_0}{\omega_0^2}\frac{\partial^2A}{\partial t^2} + k_0^3\left|A\right|^2A - 8i\frac{k_0^3}{\omega_0}\left|A\right|^2\frac{\partial A}{\partial t} - 2i\frac{k_0^3}{\omega_0}A^2\frac{\partial A^*}{\partial t} - \frac{4k_0^3}{\omega_0^2}A\frac{\partial\bar{\phi}}{\partial t} = 0 \tag{11}$$

It describes the wave evolution in space (x-evolution). The Laplace equation for $\bar{\varphi}$ and Eq. (8) also need transforming accordingly,

$$\frac{1}{C_{gr}^2}\frac{\partial^2\bar{\varphi}}{\partial t^2} + \frac{\partial^2\bar{\varphi}}{\partial z^2} = 0, \quad z \le \eta \tag{12}$$

$$\frac{\partial\bar{\varphi}}{\partial z} = -\frac{\omega_0}{2C_{gr}}\frac{\partial}{\partial t}\left|A\right|^2, \quad z = 0 \tag{13}$$

Note that the dispersion term is now explicitly written in Eq. (11), what is due to the form of the dispersion law, Eq. (6), and still describes the linear dispersion fully.

The reconstruction formulas now have the form

$$\eta(x,t) = -\frac{1}{2\omega C_{gr}}\frac{\partial\bar{\phi}}{\partial t} + \mathrm{Re}(AE) + \frac{k_0}{2}\mathrm{Re}\left(A^2E^2\right) + \frac{1}{2C_{gr}}\mathrm{Im}\left(A\frac{\partial A}{\partial t}E^2\right) + \frac{3k_0^2}{8}\mathrm{Re}\left(A^3E^3\right) \tag{14}$$

$$\varphi(x,z,t) = \bar{\varphi} - \frac{\omega_0}{k_0}\mathrm{Im}(AE)e^{k_0z} - \frac{1}{k_0}\mathrm{Re}\left[\frac{\partial A}{\partial t}E\right](1-2k_0z)e^{k_0z} - \omega_0k_0\,\mathrm{Im}\left[A\left|A\right|^2E\right]\left(\frac{3}{8}-k_0z\right)e^{k_0z} + \frac{1}{\omega_0k_0}\mathrm{Im}\left[\frac{\partial^2A}{\partial t^2}E\right] \times \left(1-kz+2k_0^2z^2\right)e^{k_0z} \tag{15}$$

The equation in form (11) is convenient for simulating the boundary problem, which appears in the case of laboratory or in situ measurements, when the data is represented by the time series measured in one point.

The wave modulation approach requires a sufficiently narrow spectrum, and; therefore, it is not always suitable for describing sea waves; meanwhile modifications of the approach might be efficient. For example, when short crested sea state is concerned, coupled equations of the Dysthe-type could be employed.

In this paper, the strongly nonlinear numerical simulation of the Euler equations is used with the purpose of verification of applicability of the Dysthe envelope model.

3 Reconstruction of the Velocity Fields

In the absolute majority of sea wave records only one of the fields, the surface elevation, is known. However, estimations of extreme wave kinematics and loads, wave dynamics, require the whole information (in particular, the velocity field). The problem, which is addressed in this section, is how to estimate the second wave field, fluid velocities, based on given surface elevation.

The wave envelope concept explicitly employs the dependence between the two fields, the surface elevation and the fluid velocity. The Hilbert transform is a primitive method for obtaining the wave envelopes, which disregards wave nonlinearity, what becomes inappropriate when rogue waves are considered. Many other approaches have been suggested (see for example Refs. [30–33]). In this study the wave envelopes are imposed according to the following approaches:

- taking into account second order wave-wave interaction
- taking into account second order and third order bound (Stokes) waves under a narrow-band assumption
- using the Creamer transform

3.1 Second Order Wave-Wave Interactions. In this approach each pair of free wave harmonics is supposed to generate bound wave components in all possible combinations,

$$\eta = \sum_{j=1}^{2} a_j\cos\theta_j + \sum_{j=1}^{2} a_j^2M_j^{[0]} + \sum_{j=1}^{2} a_j^2M_j^{[2]}\cos 2\theta_j + a_1a_2M_p\cos(\theta_1+\theta_2) + a_1a_2M_m\cos(\theta_1-\theta_2) \tag{16}$$

$$\varphi = \sum_{j=1}^{2} a_jN_j^{[1]}e^{k_jz}\sin\theta_j + \sum_{j=1}^{2} a_j^2N_j^{[2]}e^{2k_jz}\sin 2\theta_j + a_1a_2N_pe^{|k_1+k_2|z} \times \sin(\theta_1+\theta_2) + a_1a_2N_me^{|k_1-k_2|z}\sin(\theta_1-\theta_2) \tag{17}$$

Here, a_j play the roles of free wave amplitudes, and $\theta_j = \omega_jt - k_jx + \theta_j^{(0)}$ are wave phases with some constants $\theta_j^{(0)}$. The surface elevation and the velocity of each harmonic of the free waves are related according to the linear dispersion relation. Coefficients M, and N are functions of partial wavenumbers and may be found in Ref. [33]. This approach does not require the spectrum to be narrow. Though the formulas are transparent, implementation of the approach is computationally costly and did not exhibit substantial advantages when was compared with the other methods. The two other approaches discussed below are preferred in this study.

3.2 Second and Third Order Bound Waves Under the Narrow-Band Approximation. Bound (phase-locked) waves are generated due to nonresonant nonlinear wave interactions and

may be described within the high-order nonlinear Schrödinger (or Dysthe) theory (second and third order corrections will be considered), which was briefly introduced in the previous Section, and details may be found in Refs. [20,29]. This approach assumes that the wave spectrum is narrow, and the wave steepness is small. However, the comparison between the simulations within the Dysthe envelope model and the full equations of hydrodynamics in Ref. [12] showed that nonlinear solitary wave packets, which are well-captured by the envelope approach, may be quite steep (up to about $k_0H/2 = 0.2$, where H is the surface wave height) and quite short (a few individual waves). Other testimonies of the high performance of the Dysthe theory exist.

It is a strong point of this approach that it takes into account wave dispersion. In contrast to the linear approximation, the groups are not just a linear combination of Stokes waves, but are altered due to the nonlinear wave-wave interaction.

The reconstruction formulas which produce the elevation and velocity fields taking into account bound waves are given in Eqs. (9) and (10) for the case when space series is known; Eqs, (14) and (15) should be used if a time series is available. Terms up to the order $^{(2)}$ or $^{(3)}$ are retained for the second and third order approach, respectively.

3.3 Creamer Transform. The transformation which completes the free wave components by bound waves according to the Hamiltonian representation was suggested by Creamer et al. in Ref. [34]. It was shown to describe accurately the Stokes waves up to the fourth order, and thus, is of even higher order than the considered above methods, although it does not take into account wave dispersion. The reconstruction formulas for complex Fourier amplitudes of the surface elevation and surface velocity potential may be expressed in the following form (see example of application in Ref. [35])

$$\eta_k = \frac{1}{|k|}\int e^{-ikx}\left(e^{ik\eta_H} - 1\right)dx, \quad \Phi_k = \frac{1}{|k|}\int e^{ik(\eta_H - x)}\frac{\partial \Phi_H}{\partial x}dx \tag{18}$$

where for given complex-valued envelope $A(x)$ the quantities η_H and Φ_H are specified by relations

$$\begin{aligned} \eta_H &= -\mathrm{Im}(AE), \quad \Phi_H = -\hat{F}_x^{-1}\left\{\left|\frac{\omega}{k}\right|\hat{F}_x\{\mathrm{Re}(AE)\}\right\}, \\ \frac{\partial \Phi_H}{\partial x} &= -\hat{F}_x^{-1}\left\{i\,\mathrm{sgn}(k)\sqrt{g|k|}\,\hat{F}_x\{\mathrm{Re}(AE)\}\right\} \end{aligned} \tag{19}$$

(compare with expressions for $\eta^{(1)}$ and $\varphi^{(1)}$ in Eqs. (9) and (10)). Here, ω is specified according to the deep-water dispersion relation, Eq. (6), and operator $\hat{F}_x\{\cdots\}$ denotes the Fourier transform in space. The elevation and surface potential are obtained from η_k and Φ_k after the inverse Fourier transform, $\eta = \hat{F}_x^{-1}\{\eta_k\}$, $\Phi = \hat{F}_x^{-1}\{\Phi_k\}$.

The Creamer transform is originally formulated for space series. In order to apply this method to time series, the envelope is at first recalculated from the time domain to time-space domain, $A(x,t)$, within the linear framework for water wave dynamics with use of the deep-water dispersion relation,

$$A(x,t)E(x,t) = \hat{F}_t^{-1}\left\{\hat{F}_t\{A(t)E(t)\}\exp\left(-i\omega\frac{|\omega|}{g}x\right)\right\} \tag{20}$$

Then, the Creamer transform, Eqs. (18)–(19) is applied to each space series $A_H(x,t_j)$ for all t_j (the Hanning mask centered at the location of the registration, $x = 0$, is applied at this stage, which selects the area near $x = 0$ in integrals, Eq. (18)), and finally the wanted time series $\eta(x = 0, t)$ and $\Phi(x = 0, t)$ are obtained.

Figures 1–4 show examples of application of different approaches to the reconstruction of the wave fields in space (Figs. 1 and 2) and time (Figs. 3 and 4) domains. In Fig. 1, a steep Stokes wave is shown ($k_0H/2 = 0.3$, where H is the wave height): the surface elevation, surface velocity potential and their Fourier spectra, represented by different envelope approaches. The solid green curve gives the "exact" Stokes wave solution, found numerically with use of the conformal representation of the Euler equations. The second order wave-wave interaction curves coincide with the second order NLS theory for narrow-banded waves. It follows from Figs. 1(*b*) and 1(*d*) that although the Creamer transform deviates from the exact solution, it has wider spectrum and potentially may describe steeper wave crests.

Figure 2 shows a similar comparison for the case of a solitary wave envelope, which is the analytic soliton solution of the NLS equation. Such long-living nonlinear wave groups have been observed in fully nonlinear numerical simulations [11,12] and also in laboratory tests [15]. Note that although the deviation between the surface elevation profiles obtained from different envelope approaches is invisible (Fig. 2(*a*), the distinctions between the vertical velocities in Fig. 2(*b*) and spectral tails in Fig. 2(*c*) are obvious.

By the moment, the reconstruction formulas were applied with the purpose to produce the bound wave corrections for a given wave envelope. The inverse problem, when the envelope is obtained on the basis of known wave elevation, gives the way to find fluid velocities. In laboratory and in situ experiments it is most typical to deal with time series. Therefore to test it, use was made below of the formulation of reconstruction formulas (the high-order NLS theory and the Creamer approach) which is capable to deal with time series.

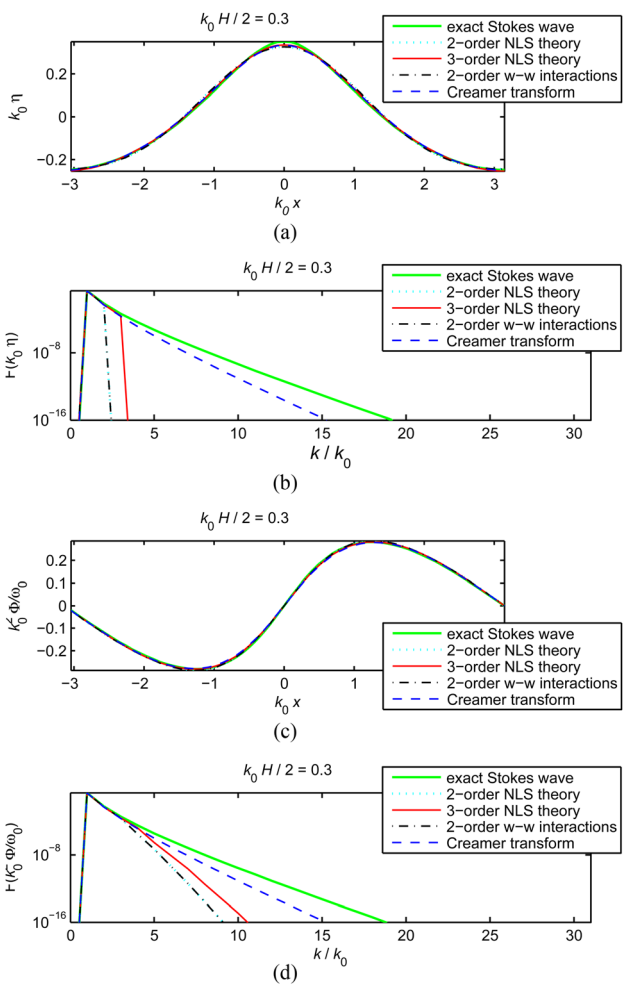

Fig. 1 Comparison of a Stokes wave ($k_0H/2 = 0.3$) reconstructed within different frameworks: the wave profile and the corresponding Fourier spectrum (*a*) and (*b*), and the surface velocity potential and its Fourier spectrum (*c*) and (*d*)

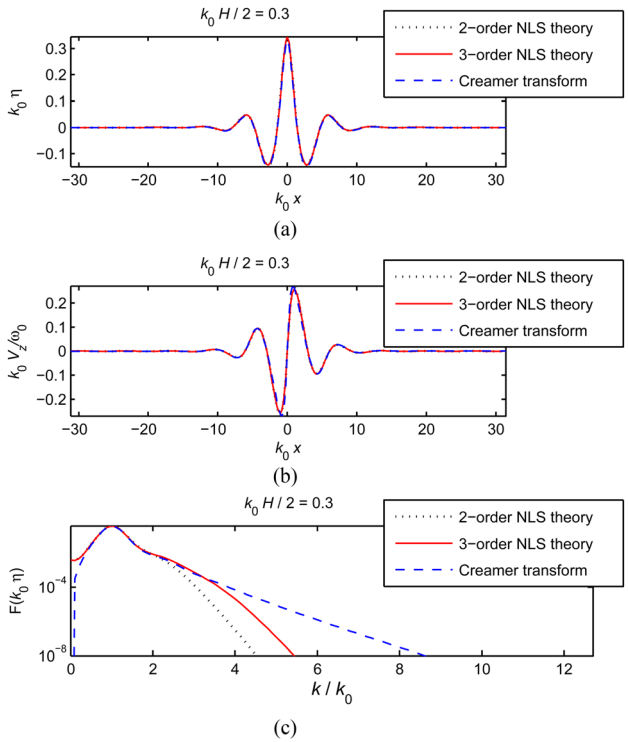

Fig. 2 Reconstruction of a solitary nonlinear wave group (steepness $k_0H/2 = 0.3$) within different frameworks: the wave profile (*a*), vertical fluid velocity at the water surface (*b*), Fourier spectrum of the surface elevation (*c*)

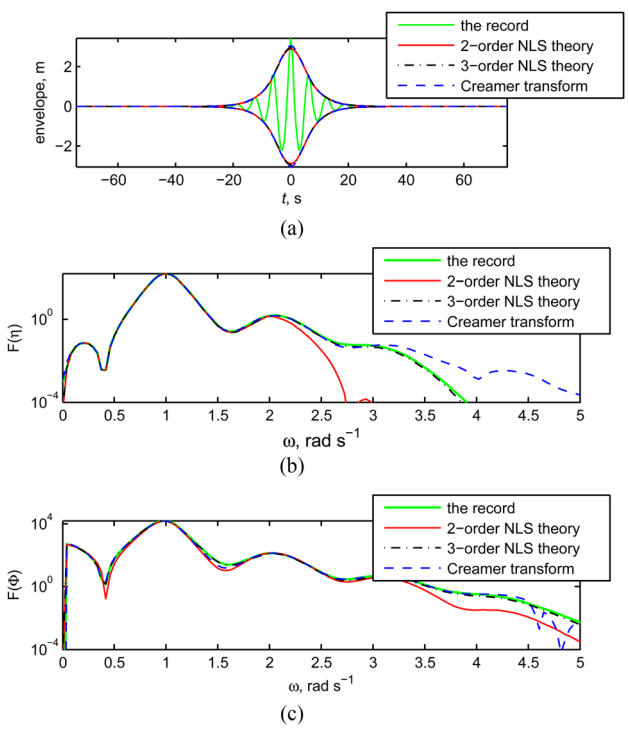

Fig. 3 Test of the reconstruction procedures for time series. The input time series is the NLS solitary group (peak frequency 1 rad/s, steepness $k_0H/2 = 0.3$, with bound waves of three orders). Panel (*a*): the target time series and reconstructed envelopes. Panels (*b*) and (*c*): Fourier spectra in semilogarithmic scales for the surface displacement and surface velocity potential.

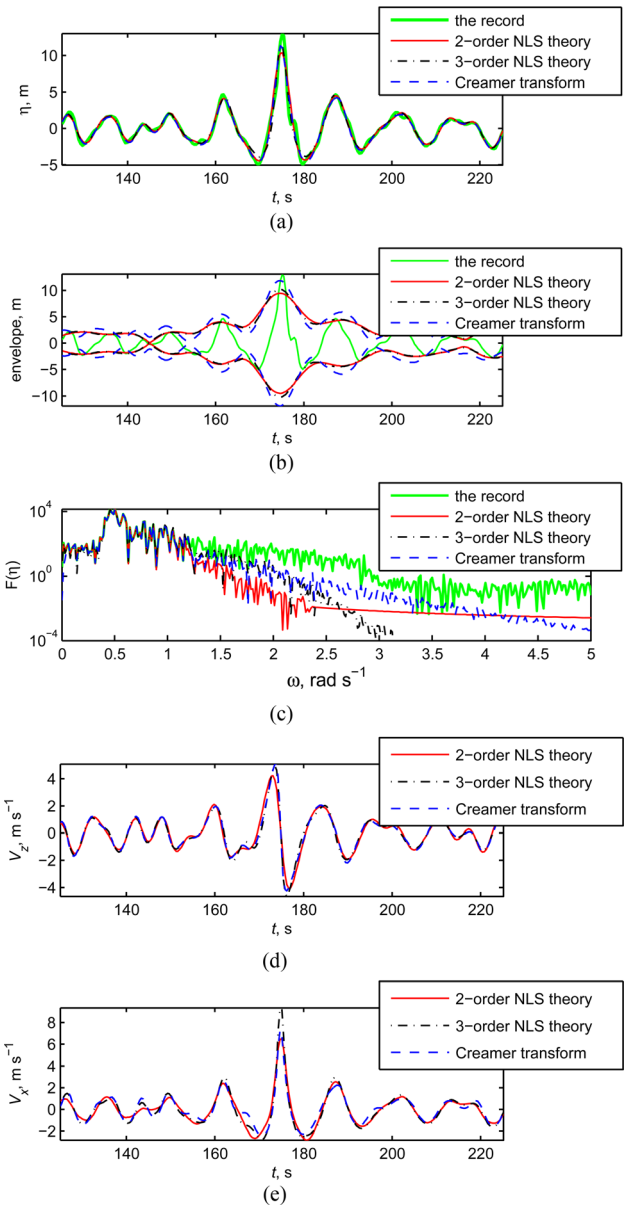

Fig. 4 Different wave envelope approaches applied to the time series NA199711200151 from the North Alwyn platform: original and reconstructed surface elevation (*a*), wave envelopes (*b*), Fourier spectrum of the surface elevation (*c*), vertical (*d*), and horizontal (*e*) fluid velocities at the water surface

The first test of such procedure is shown in Fig. 3, when, similarly to Fig. 2, the time series of surface elevation described by the NLS envelope soliton is used as the input data. The wave profile is produced for the soliton with characteristic steepness 0.3 taking into account third order bound wave corrections, Eq. (9). The time series of the surface elevation is the only information which is used for the reconstruction of the envelope and then the velocity potential. An iterative numerical procedure is used to adjust the wanted envelope function with strategy to minimize the mean square difference between the target and reconstructed series of surface elevations (maximum ten iterations is allowed). A frequency cut-off is applied to the envelope, so that it is admitted to occupy the spectral domain in the range $(-\omega_0, +\omega_0)$, where the carrier wave frequency, ω_0, is also adjusted by the iterative procedure.

The difference between the target and reconstructed surface elevations is almost invisible (it is most noticeable near the maximum wave crest, not shown); the errors of the reconstruction are

up to about 2.5%. The difference between the envelope shapes is somewhat easier to observe and is shown in Fig. 3(*a*); it is most pronounced near the group maximum; the amplitude of the wave envelope increases in the order: second order, third order NLS theories, and the Creamer approach.

It is natural, that the third order NLS theory provides the best agreement with the target wave (see Figs. 3(*b*) and 3(*c*)). The application of the Creamer transform results in longer spectrum tail for the surface elevation, while the second order NLS theory underestimated the spectrum tail magnitude.

Finally, different approaches are applied to the in situ record NA199711200151 as shown in Fig. 4. In the discussed ten time series from the North Sea the extreme waves are single waves or intense wave groups (see time series in Figs. 6 and 7 below). The crest amplitudes are from 8.7 to 13.2 m, the mean wave lengths are estimated within the range 140–180 m. Thus, the waves are strongly nonlinear, and the peak wave steepness, k_0A_{cr} is close to the breaking limit. Each time series is represented by a 20-min sequence of surface elevations with good resolution (5 Hz). The details of the measurements and conditions may be found in Ref. [25].

An extract of the recorded time series NA199711200151 is shown in Fig. 4(*a*) and 4(*b*) in a large scale (the green solid line). It contains a wave of 18.2 m height with the crest 13.2 m, with the amplification factor $H_{\max}/H_s = 2.31$. The mean wave period in the record is about 10 s.

The resulting envelopes (absolute values of the complex amplitudes, $\pm|A(t)|$) are plotted in Fig. 4(*b*). The reconstructed surface elevations are shown in Fig. 4(*a*) by different lines, and the corresponding Fourier spectra—are shown in Fig. 4(*c*). Although the envelopes provided by the second and third order NLS theories look quite similar, the differences between the surface elevation shapes (Fig. 4(*a*)) and the reconstructed velocities (Figs. 4(*e*) and 4(*d*)) are noticeable. The envelopes obtained through the approaches may be rather different, as well seen in Fig. 4(*b*), and the horizontal velocities also differ significantly (Fig. 4(*e*)). All the approaches result in Fourier spectra with the tails which decay significantly faster than it is measured in the sea (Fig. 4(*c*)).

In the numerical experiments described below the third order bound wave correction formulas are employed.

4 Reconstruction of Rogue Events

In most cases the in situ registrations are represented by the time series of the water surface displacement, retrieved in one point. Even if the fluid velocity is obtained at the location of the measurement by virtue of the described above approaches, the information on the wave history and further evolution is important. This information can discover even more extreme events nearby the point of registration, and can answer the question on the rogue wave life time. In this section the complete dynamics of the rogue wave in time and space is reconstructed by means of numerical simulations of dynamical equations. The simulations are performed upstream and downstream the wave evolution under the assumption of unidirectional wave propagation.

In the previous study [22–24] several rogue wave events recorded at the North Alwyn platform and Draupner platform, and also recorded in the Black Sea, were simulated within the framework of approximate equations for wave modulations. It was found that the amplitude criterion on rogue waves $H/H_s > 2$, where H_s is the significant wave height remains satisfied for up to a hundred seconds (rogue wave lifetime).

The present paper aims at some sort of verification of the weakly nonlinear simulations by the Dysthe equation. When a time series of a rogue wave is available, models for the x-evolution (like Eq. (11)) are most suitable. However, the primitive equations of hydrodynamics, Eqs. (1)–(4) describe the evolution *in time*, and therefore a direct use of the strongly nonlinear codes is impossible. To perform validation of the approximate simulations, the following strategy is employed, as described below (see the illustration in Fig. 5):

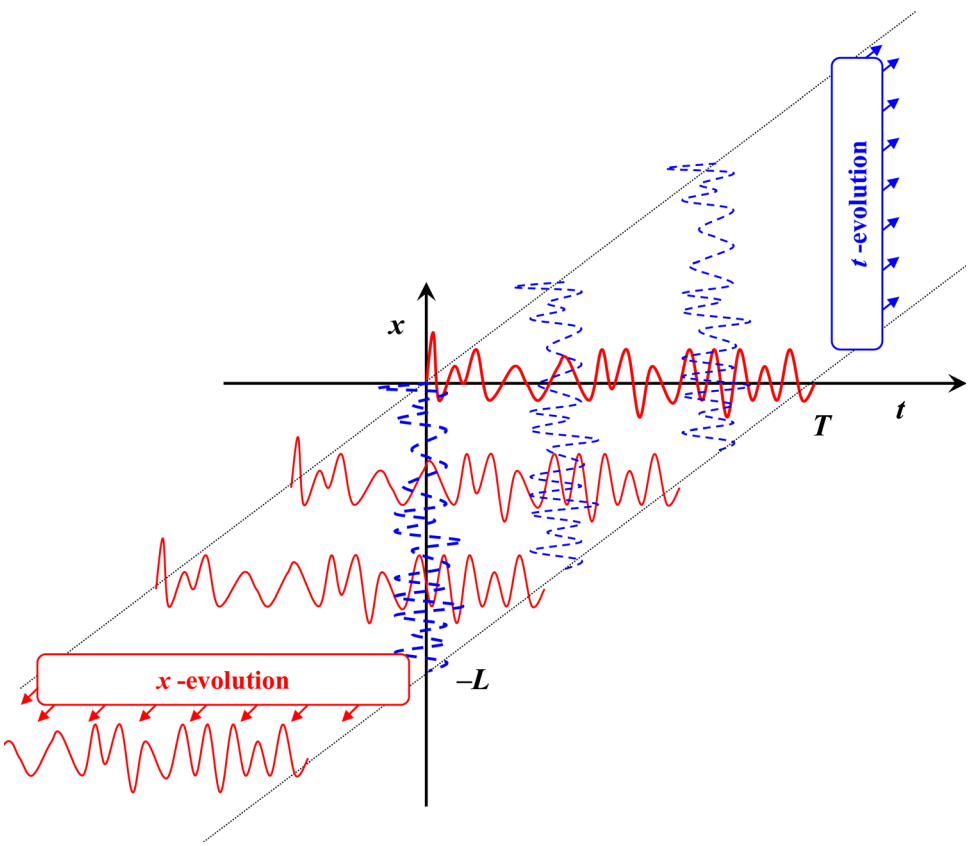

Fig. 5 Explanation diagram for the upstream *x*-evolution and forward *t*-evolution

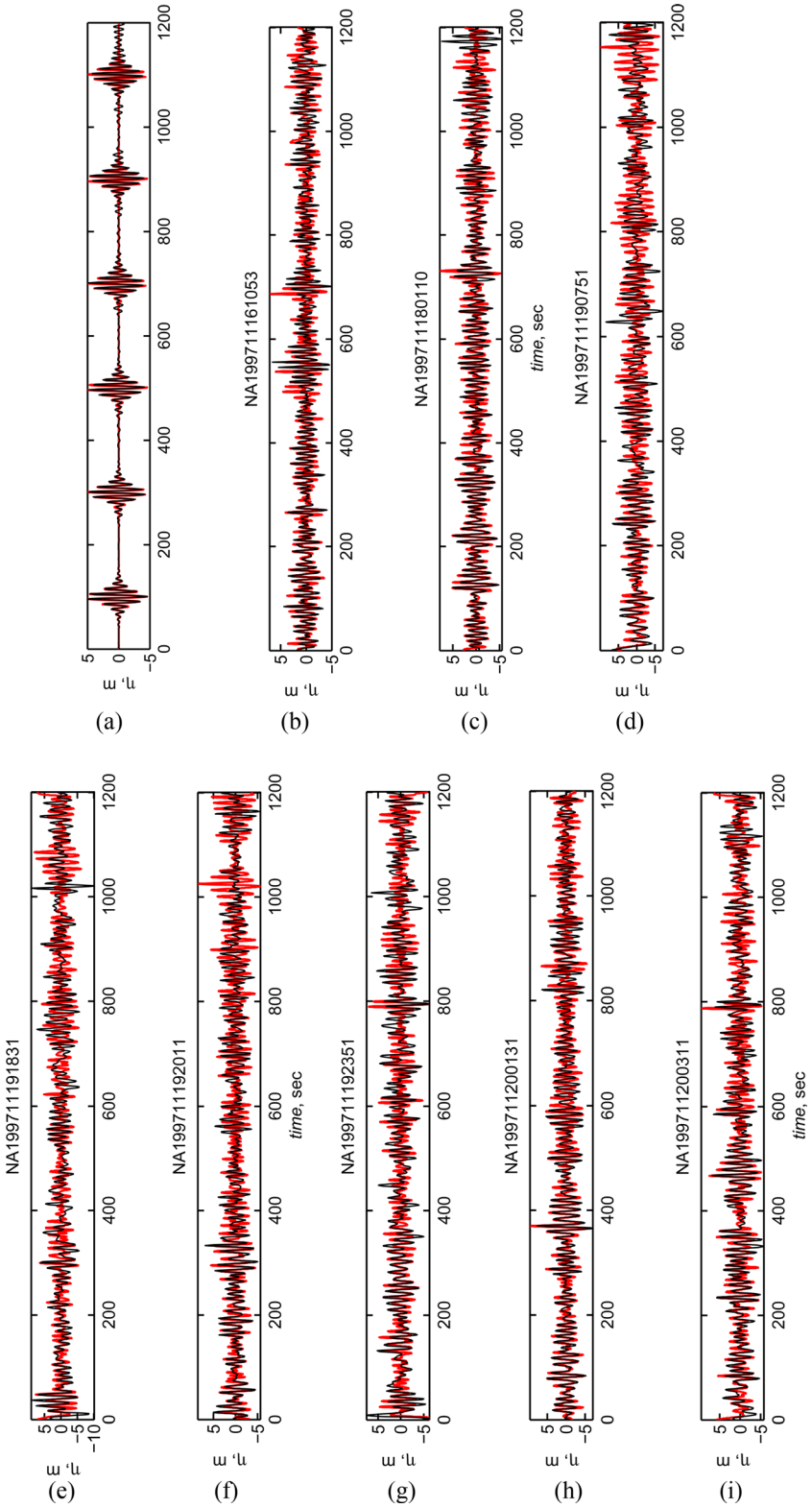

Fig. 6 Verification of the combined use of the spatial and temporal versions the Dysthe equations. The thick red line is the initial condition, the thin black line is the recovered time series: a train of solitary waves (*a*), and the time series from the North Alwyn platform (*b*)–(*i*), see record codes above the figures.

(1) The wave envelope $A(t)$ is reconstructed on the basis of the registered time series $\eta_{rec}(t)$ (shown in Fig. 5 by a red solid line at $x = 0$, $0 < t < T$) with the third order Dysthe theory, Eq. (14).
(2) The envelope $A(x = 0, t)$ is simulated upstream by means of the Dysthe equation (11) (backward x-evolution) up to location $x = -L$ (see the sequence of waves by red solid lines in Fig. 5). Hence, the wave fields $A(x, t)$, $\eta(x, t)$, and $\Phi(x, t)$ are obtained in some domain (x, t), and the initial conditions $A(x, t = 0)$, $\eta(x, t = 0)$ and $\Phi(x, t = 0)$ may be formulated (shown by the blue broken line in Fig. 5 at $t = 0$, $0 < x < L$).

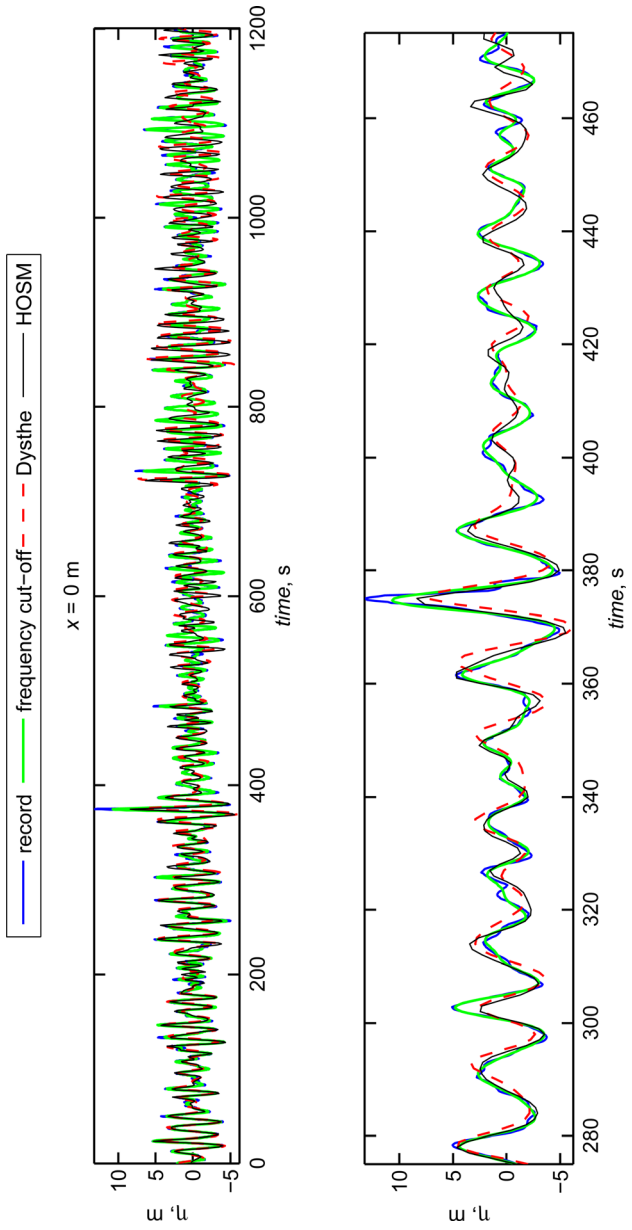

Fig. 7 A reconstruction of the wave record NA199711200151. The in situ recorded wave ("record"), the high-frequency filtered time-series ("frequency cut-off"), simulations of the Dysthe equation and the strongly nonlinear HOSM ($M=6$) simulation. The whole time series is given in panel (*a*), and the rogue wave event is shown in a larger scale in panel (*b*).

The third step (forward t-simulation, represented by the sequence of waves given in blue broken lines in Fig. 5) is undertaken in two different ways,

(3) The wave envelope $A(x, t=0)$ is simulated by means of the Dysthe equation (8) downstream until $t=T$.
(4) Alternatively to step (3), the couple of fields $\eta(x, t=0)$ and $\Phi(x, t=0)$ is used as the initial condition for the Euler equations (1)–(4), and are simulated downstream by means of the HOSM method until $t=T$.

One of the results of this loop of backward x-simulation and forward t-simulation, is the recovered surface elevation $\eta(t)$ at the point of the in situ measurement, $x=0$. The recovered elevation, theoretically, should coincide with the in situ recorded values, $\eta(t)=\eta_{\text{rec}}(t)$, what in fact does not happen. The difference obtained is not due to the numerical errors, but due to the fact that different wave models were solved upstream and downstream wave propagation. The evolution in time and evolution in space Dysthe models (7) and (11) are *asymptotically* close under the assumptions of small nonlinearity and dispersion. Therefore, they describe wave evolution with some difference which is admitted by the asymptotic approach (of order ε^4, where ε is the characteristic wave steepness). In the extraordinary situation of steep rogue waves the asymptotic expansions may become invalid; hence, the difference between the two models is not surely small. In comparison with the employed Dysthe equation, the HOSM describes differently the effects of strong nonlinearity and also may result in a different shape of the reconstructed wave.

Examples of the original and recovered time series are shown in Fig. 6, when the downstream simulation is performed within the Dysthe theory framework, i.e., steps (1), (2), and (3) are undertaken. The red solid lines show the initial surface displacements, η_{rec}, (time series of 1200 s duration at location $x=0$), while the thin black lines are the results of the upstream x-simulation of the Dysthe equations (11) up to $x\approx -9200$ m, and then the forward t-simulation of the Dysthe equations (7) up to $t=1200$ s.

Panel (*a*) in Fig. 6 demonstrates the sample when the initial wave field is specified in the form of a sequence of envelope solitons (similar to shown in Fig. 3) with the characteristic steepness $k_0H/2\approx 0.2$ and wave period 10 s. It may be easily realized from the sketch in Fig. 5, that waves with smaller t in the recorded time series during the loop of the simulations upstream and return eventually pass a smaller distance, and therefore, should be less affected by the difference in governing evolution equations; hence should be restored with a better performance. Results shown in Fig. 6(*a*) confirm this expectation: after the loop of simulations waves registered at small t are reproduced almost perfectly, while the waves which correspond to longer simulation distances exhibit some difference between the original and recovered wave shapes.

Figures 6(*b*)–6(*i*) show similar results, when the rogue wave records from the North Alwyn platform are used as the input data, $\eta_{\text{rec}}(t)$.

Because the equations are solved numerically with the help of the discrete Fourier transform, periodic boundary conditions are imposed, which alter the actual data. Therefore, some part of the records near $t\approx 0$ and $t\approx 1200$ s for $x=0$ is simulated *a fortiori* in a wrong way and cannot be reconstructed by this approach. This effect may excuse the manifest distinction between surface displacements at, e.g., the right side of Fig. 6(*c*).

The difference between the original surface elevation, and the recovered data may be provided either by the terms which are not taken into account by the Dysthe equations or due to the strongly nonlinear nature of the waves, and thus cancellation of the formal range of applicability of the approximate model and hence, inconsistency of the spatial and temporal versions of the Dysthe equations.

To see the role of the strong nonlinearity we perform the forward simulation from $t=0$ to $t=1200$ s by means of the strongly nonlinear high order spectral method for the Euler equations. We set the nonlinearity parameter $M=6$ (resolution of up to 7-wave interactions), see Ref. [26]. The result of the simulation is shown in Fig. 7 for the record NA199711200151.

The measurement of the sea wave (the solid blue line in Fig. 7) was first filtered (the solid green line) to cut off the high-frequency wave components which definitely cannot be captured by the third order bound wave corrections. It may be seen that this cut-off reduces the rogue wave amplitude significantly.

The wave profile after the upstream and thereupon forward simulation within the framework of the Dysthe equation (steps (1), (2) and (3)) is shown in Fig. 7 by the dashed red curve. When the forward t-simulation is performed within the frameworks of the fully nonlinear equations (steps (1), (2), and (4)), the recovered wave elevation is shown in Fig. 7 by the black solid line. In general, all these curves are rather close around the moment of the extreme event. The recovered extreme waves both exhibit smaller amplitudes than the initial wave, although the fully nonlinear simulation results in a bigger wave.

It follows from the analysis of Fig. 7, that the considered extreme wave dynamic is in fact rather well captured by the Dysthe model, although the extreme wave amplitude is underestimated by all the applied models. However, the reconstruction procedures could not reproduce the recorded waves for the time intervals larger than about 10 min (see Figs. 6 and 7), what is less than the typical duration of a time series (20 min).

5 Conclusion

The problem of reconstruction of an abnormal event in the major part consists of restoring the field of the fluid velocity on the basis of incomplete information represented by the time series of the surface elevation retrieved at a single point. To proceed this way, the waves are typically assumed to be freely propagating and unidirectional. Besides these assumptions other simplifications are usually involved (weakly nonlinear or/and narrow-banded waves) to enable reconstruction of the nonlinear velocity field.

In the paper three different approaches are considered: the second order nonlinear corrections due to wave-wave interactions; the second and third order corrections in the assumption of narrow-banded waves; and the Creamer transform which is a fourth order approach. Ten wave records of abnormal waves retrieved on the North Alwyn platform from the North Sea are used to test the envelope approaches. The sea conditions correspond to relatively deep water.

Some differences between these approaches are highlighted which may result in distinct kinematic and dynamical properties of extreme waves, although the preferable approach is not evident at the stage. All the tested approaches could not reproduce the wide wave spectrum measured in situ, and thus, the simulated extreme wave is always somewhat smaller than the measured one.

This paper shows that the rogue wave evolution may be reconstructed in a realistic way by means of numerical simulations. The approach is validated by means of cross-simulations of different Dysthe models, and also with the help of the fully nonlinear simulation of the Euler equations. The adopted here method differs from the one developed and applied by Clauss et al. [21] in the part, that the wave dynamics is permitted to be significantly nonlinear, so that the wave spectrum may change. Thus, potentially the present approach may have a wider range of applicability.

It is demonstrated that in some cases the approximate NLS (Dysthe) theory may be suitable for the description of rogue events, although the reconstructed extreme wave is smaller in height. The reconstructed steep wave dynamics becomes inadequate for a large distance/time of wave propagation. This limit is estimated to be about 10 min, what corresponds to about 60 wave periods.

Some time series of the abnormal events could not be described well by the envelope approach: the difference between the original time series and the simulated upstream and thereupon forward waves is found unacceptable. In some cases the forward simulation could not be performed by means of the HOSM due to numerical instability, which may be attributed to the wave breaking.

The revealed mismatches between input and reconstructed surface elevations may prove the importance of strongly nonlinear effects of wave dynamics, including wave breaking, and also importance of the effects of wave directionality. The wave breaking effect makes the description much more difficult and the results which will be obtained for this case are expected to be generally less robust. The accounting for wave directionality obviously increases the freedom in formulating the initial conditions, and naturally decreases the reliability of the reconstruction procedure. Moreover, a new dimension may change the strongly nonlinear wave dynamics drastically, as new wave-wave resonances become allowed, and 3D wave instabilities may act. With this concern it is interesting to point out the approach by Adcock and Taylor [37], where the method to estimate the directional spreading is suggested, which employs the peculiarities of bound wave components.

The particular cases, when the reconstruction of the rogue wave dynamics exhibit robust and steady results are of a high interest and the paper presents such an example.

Acknowledgment

The research has received funding from the EC's Seventh Framework Programme FP7-SST-2008-RTD-1 project EXTREME SEAS – Design for Ship Safety in Extreme Seas (http://www.mar.ist.utl.pt/extremeseas/) under Grant agreement No 234175. AS and EP acknowledge RFBR Grants Nos. RFBR11-02-00483, RFBR11-05-00216, and RFBR12-05-33087. Research by AS is financed by the EC's Seventh Framework Programme FP7-PEOPLE-2009-IIF under Grant agreement No 909389. EP is grateful for partial support from the Volkswagen Foundation.

References

[1] Kharif, C., and Pelinovsky, E., 2003, "Physical Mechanisms of the Rogue Wave Phenomenon," Eur. J. Mech. B/Fluids, **22**, pp. 603–634.
[2] Dysthe, K., Krogstad, H. E., and Müller, P., 2008, "Oceanic Rogue Waves," Annu. Rev. Fluid Mech., **40**, pp. 287–310.
[3] Kharif, C., Pelinovsky, E., and Slunyaev, A., 2009, *Rogue Waves in the Ocean*, Springer-Verlag, Berlin.
[4] Rosenthal, W., Lehner, S., Dankert, H., Guenther, H., Hessner, K., Horstmann, J., Niedermeier, A., Nieto-Borge, J. C., Schulz-Stellenfleth, J., and Reichert, K., 2003, "Detection of Extreme Single Waves and Wave Statistics," MaxWave. Rogue Waves – Forecast and Impact on Marine Structures, Final Meeting and Workshop. Working Group Reports.
[5] Lawton, G., 2001, "Monsters of the Deep (The Perfect Wave)," New Scientist, **170**(2297), pp. 28–32. Available at: http://www.newscientist.com/article/mg17022974.900-monsters-of-the-deep.html
[6] Guedes Soares, C., and Teixeira, A. P., 2001, "Risk Assessment in Maritime Transportation," Reliab. Eng. Syst. Saf., **74**, pp. 299–309.
[7] Toffoli, A., Lefevre, J. M., Bitner-Gregersen, E., and Monbaliu, J., 2005, "Towards the Identification of Warning Criteria: Analysis of a Ship Accident Database," Appl. Ocean Res., **27**, pp. 281–291.
[8] Guedes Soares, C., Bitner-Gregersen, E., and Antão, P. 2001, "Analysis of the Frequency of Ship Accidents Under Severe North Atlantic Weather Conditions," *Proceedings of the Conference on Design and Operation for Abnormal Conditions II*, RINA, London, pp. 221–230.
[9] Bitner-Gregersen, E., Guedes Soares, C., and Silvestre, A., 1998, "On the Average Wave Steepness," *Proceedings of the Ocean Wave Kinematics, Dynamics and Loads on Ship Structures (Wave'98)*, ASCE, Houston, TX, pp. 513–520.
[10] Guedes Soares, C., Fonseca, N., and Pascoal, R., 2008, "Abnormal Wave Induced Load Effects in Ship Structures," J. Ship Res., **52**(1), pp. 30–44. Available at: http://www.ingentaconnect.com/content/sname/jsr/2008/00000052/00000001/art00003#expand/collapse
[11] Dyachenko, A. I., and Zakharov, V. E., 2008, "On the Formation of Freak Waves on the Surface of Deep Water," JETP Lett., **88**, pp. 307–311.
[12] Slunyaev, A. V., 2009, "Numerical Simulation of "Limiting" Envelope Solitons of Gravity Waves on Deep Water," JETP, **109**, pp. 676–686.
[13] Chabchoub, A., Hoffmann, N. P., and Akhmediev, N., 2011, "Rogue Wave Observation in a Water Wave Tank," Phys. Rev. Lett., **106**, p. 204502.
[14] Chabchoub, A., Hoffmann, N., Onorato, M., Slunyaev, A., Sergeeva, A., Pelinovsky, E., and Akhmediev, N., 2012, "Observation of a Hierarchy of Up to Fifth-Order Rogue Waves in a Water Tank," Phys. Rev. E, **86**, p. 056601.
[15] Slunyaev, A., Clauss, G. F., Klein, M., and Onorato, M., 2013, "Simulations and Experiments of Short Intense Envelope Solitons of Surface Water Waves," Phys. Fluids, **25**, p. 067105.
[16] Trulsen, K., 2001, "Simulating the Spatial Evolution of a Measured Time Series of a Freak Wave," *Proc. of the Workshop "Rogue Waves 2000,"* M. Olagnon and G. A. Athanassoulis, eds., Ifremer, Brest, France, pp. 265–274.
[17] Dysthe, K. B., 1979, "Note on a Modification to the Nonlinear Schrödinger Equation for Application to Deep Water Waves," Proc. R. Soc. London, Ser. A, **369**, pp. 105–114.
[18] Trulsen, K., and Dysthe, K. B., 1996, "A Modified Nonlinear Schrödinger Equation for Broader Bandwidth Gravity Waves on Deep Water," Wave Motion, **24**, pp. 281–289.
[19] Trulsen, K., Gudmestad, O. T., and Velarde, M. G., 2001, "The Nonlinear Schrödinger Method for Water Wave Kinematics on Finite Depth," Wave Motion, **33**, pp. 379–395.
[20] Trulsen, K., 2006, "Weakly Nonlinear and Stochastic Properties of Ocean Wave Fields: Application to an Extreme Wave Event," J. Grue and K. Trulsen, eds., *Waves in Geophysical Fluids: Tsunamis, Rogue Waves, Internal Waves and Internal Tides*, CISM Courses and Lectures No. 489, Springer, New York.
[21] Clauss, G. F., and Klein, M., 2009, "The New Year Wave: Spatial Evolution of an Extreme Sea State," ASME J. Offshore Mech. Arct. Eng., **131**, p. 041001.
[22] Divinsky, B. V., Levin, B. V., Lopatukhin, L. I., Pelinovsky, E. N., and Slyunyaev, A. V., 2004, "A Freak Wave in the Black Sea: Observations and Simulation," Dokl. Earth Sci., **395A**, pp. 438–443.
[23] Slunyaev, A., Pelinovsky, E., and Guedes Soares, C., 2005, "Modeling Freak Waves From the North Sea," Appl. Ocean Res., **27**, pp. 12–22.

[24] Slunyaev, A., 2006, "Nonlinear Analysis and Simulations of Measured Freak Wave Time Series," Eur. J. Mech. B/Fluids, **25**, pp. 621–635.
[25] Guedes Soares, C., Cherneva, Z., and Antão, E., 2003, "Characteristics of Abnormal Waves in North Sea Storm Sea States," Appl. Ocean Res., **25**(6), pp. 337–344.
[26] West, B. J., Brueckner, K. A., Janda, R. S., Milder, D. M., and Milton, R. L., 1987, "A New Numerical Method for Surface Hydrodynamics," J. Geophys. Res., **92**, pp. 11803–11824.
[27] Zakharov, V., 1968, "Stability of Periodic Waves of Finite Amplitude on a Surface of Deep Fluid," J. Appl. Mech. Tech. Phys., **9**, pp. 190–194.
[28] Clamond, D., Francius, M., Grue, J., and Kharif, C., 2006, "Long Time Interaction of Envelope Solitons and Freak Wave Formations," Eur. J. Mech. B/Fluids, **25**, pp. 536–553.
[29] Slunyaev, A. V., 2005, "A High-Order Nonlinear Envelope Equation for Gravity Waves in Finite-Depth Water," JETP, **101**, pp. 926–941.
[30] Veltcheva, D., Cavaco, P., and Guedes Soares, C., 2003, "Comparison of Methods for Calculation of the Wave Envelope," Ocean Eng., **30**, pp. 937–948.
[31] Veltcheva, D., and Guedes Soares, C., 2007, "Analysis of Abnormal Wave Records by the Hilbert Huang Transform Method," J. Atmos. Oceanic Technol., **24**(9), pp. 1678–1689.
[32] Cherneva, Z., and Guedes Soares, C., 2008, "Non-Linearity and Non-Stationarity of the New Year Abnormal Wave," Appl. Ocean Res., **30**, pp. 215–220.
[33] Petrova, P. G., Arena, F., and Guedes Soares, C., 2011, "Space-Time Evolution of Random Wave Groups With High Waves Based on the Quasi-Determinism Theory," Ocean Eng., **38**, pp. 1640–1648.
[34] Dalzell, J. F., 1999, "A Note on Finite Depth Second-Order Wave-Wave Interactions," Appl. Ocean Res., **21**, pp. 105–111.
[35] Creamer, D. B., Henyey, F., Schult, R., and Wright, L., 1989, "Improved Linear Representation of Ocean Surface Waves," J. Fluid Mech., **205**, pp. 135–161.
[36] Taylor, P. H., Ohl, C.O.G., and Sauvee, J., 1999, "Focused Wave Groups I: Local Structure, Kinematics, and the Creamer Transform," Proc. OMAE 1999, Paper No. OMAE99/S&R-6461.
[37] Adcock, T.A.A., and Taylor, P. H., 2009, "Estimating Ocean Wave Directional Spreading From an Eulerian Surface Elevation Time History," Proc. R. Soc. London, Ser. A, **465**, pp. 3361–3381.